Responses of dynamic penetrometers according to hammer weight and drop height

Geunwoo Park[1], *Namsun* Kim[1], *Dong-Ju* Kim[1], *Sang Yeob* Kim[2] and *Jong-Sub* Lee[1#]

[1]*Korea University, School of Civil, Environmental and Architectural Engineering, 145, Anam-ro, Seongbuk-gu, Seoul, 02841, Republic of Korea*
[2] *Konkuk University, Department of Fire and Disaster Prevention, 268, Chungwon-daero, Chungju-si, Chungcheongbuk-do, 27478, Republic of Korea*
[#]*Corresponding author: jongsub@korea.ac.kr*

ABSTRACT

This study characterizes the dynamic responses of hammer weight and drop height in dynamic penetration tests. The tests were conducted using an instrumented dynamic cone penetrometer (IDCP) to obtain the dynamic responses during penetration. Various hammer weight and drop height types were used at a fixed potential energy of 45.1 N·m. The measured compression stresses and transferred energies into the rod head and cone tip were analyzed for hammer weight and drop height. The compression stress at the rod head varied with the hammer weight and drop height, whereas the compression stress at the cone tip is irrelevant to the hammer weight or drop height. In addition, the transferred energies into the rod head and cone tip increased as the hammer weight increased but decreased as the drop height increased. This study demonstrates that hammer weight and drop height should be considered when the characteristic of subsurface is profiled using dynamic penetrometer.

Keywords: drop height; dynamic response; hammer weight; instrumented dynamic cone penetrometer

1. Introduction

Dynamic penetration tests were conducted to characterize the ground strength. Standard penetration test (SPT) is a representative test using dynamic blow. The SPT hammer weight and drop height were standardized to ensure the constant potential energy of the dynamic blow. Results of SPT were used for evaluating the engineering properties of ground. In some cases, dynamic penetration test were conducted using non-standardized hammer weight and drop height. To correct the results of non-standardized SPT, formulas were suggested (Burmister, 1948). The number of blows for 30 cm increases as hammer weight and drop height increase. The ratio of transferred energy to potential energy is linearly proportional to the drop height (Youd et al., 2008).

In some cases, a dynamic cone penetrometer (DCP) has been used for ground characterization due to its simplicity and high mobility. The hammer weight and drop height of the DCP were standardized as 8 kg and 575 mm, respectively. However, energy loss lead to the inaccuracy of the DCP results. Thus, an instrumented dynamic cone penetrometer (IDCP) was developed to consider the energy loss (Lee and Byun, 2020). Dynamic responses are obtained using energy module in the IDCP and transferred energy is calculated. The potential energy of hammer influences on the transferred energy, therefore, consistency of energy is important for ground characterization. In addition, the dynamic responses vary with the end boundary conditions.

In this study, the dynamic responses were obtained and analysed using the IDCP in free- and fixed-end boundary conditions. The IDCP tests were conducted at compacted soils and stainless-steel plate. This paper first introduces background theory of the IDCP and effect of hammer weight and drop height. Subsequently, an experimental study and result are represented. Finally, the results of the IDCP tests are analyzed.

2. Background theory

2.1. Instrumented dynamic cone penetrometer

A DCP, which is a portable dynamic penetrometer, was standardized to characterize the strength of subsurface (Scala, 1956). Standardized hammer weight and drop height of DCP are 8 kg and 0.575 m, respectively. The potential energy of DCP is calculated as 45.13 N·m by multiplication of gravitational acceleration, hammer weight and drop height. The penetration depth of DCP is recorded as DCP index (DCPI). The DCPI was used to estimate the ground engineering properties (George et al., 2009; Malek et al., 2020). However, inconsistent dynamic blows are caused by the energy loss; thus, the results of DCP are inaccurate.

An IDCP was developed to compensate for inaccurate DCP results (Byun and Lee, 2013). The hammer weight and drop height of the IDCP are identical to those of the standard DCP, however, a hammer weight of 12 kg with an identical drop height was used in some cases to improve the drivability (Kim and Lee, 2020; Park et al., 2023). The measurement system for the IDCP is illustrated in Fig. 1. The IDCP probe and energy module anvil for measurement of dynamic responses are located at a cone tip and rod head. Accelerometers and load cells

are installed inside the IDCP probe and energy module anvil to protect the sensors. For each dynamic blow, the IDCP index (IDCPI) is calculated by the penetration depth.

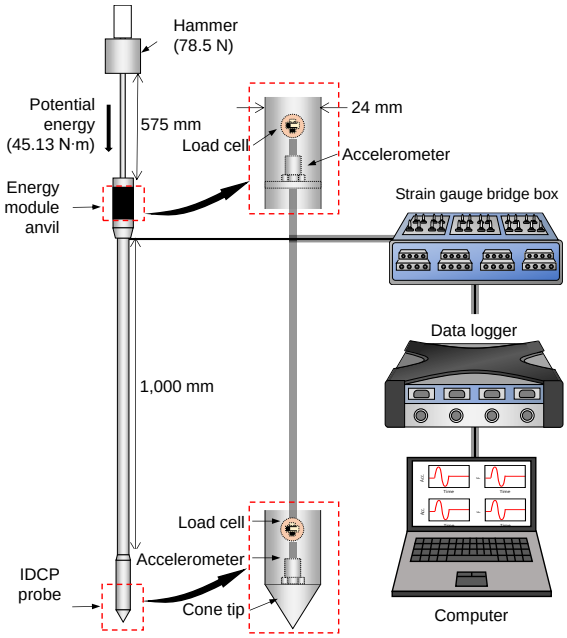

Figure 1. Measurement system of instrumented dynamic cone penetrometer.

2.2. Effect of hammer weight and drop height

The compression stress at the rod head is calculated by dividing the compression force by the cross-sectional area (A) of the rod; additionally, it is expressed by the elastic modulus (E), velocity of the compression wave (c), gravitational acceleration (g), and drop height (h) as follows:

$$\sigma_i = \frac{F}{A} = \frac{1}{A}\frac{EA}{c}v = \frac{E}{c}v = \frac{E}{c}\sqrt{2gh} \qquad (1)$$

where σ_i, F, and v denote the compression stress, compression force, and particle velocity, respectively. Thus, the σ_i increases with the h as expressed in Eq. (1).

For dynamic blow, the equilibrium equation of force at a specific location can be derived by compression stress at a specific location (σ), cross-sectional area (A), hammer weight (W_H), and acceleration (a) as follows:

$$\sigma A + W_H a = 0 \qquad (2)$$

The a is the differentiation of v with respect to time (t), and v can be expressed as the product of c and strain. Subsequently, the first order ordinary differential equation (ODE) is as follows:

$$\sigma A + \frac{W_H c}{E}\frac{d\sigma}{dt} = 0 \qquad (3)$$

As separable ODE among the first-order ODE, the equation can be rearranged with rod weight (Wg) and time factor (α) for σ as follows:

$$\sigma = \sigma_i e^{-\frac{W_R}{W_H}\alpha} = \frac{E}{c}\sqrt{2gh}\, e^{-\frac{W_R}{W_H}\alpha} \qquad (4)$$

Thus, drivability, which is determined by the compression stress, is theoretically affected by the hammer's weight and height.

3. Experimental study

3.1. Site description

Dynamic cone penetration tests using the IDCP were conducted at compacted soils in the embankment (three sites) to measure the IDCPI and on a stain-less steel plate to obtain the dynamic responses. First, five types of hammer weight (4, 8, 12, 16, and 24 kg) were used for dynamic blow with an adjusted drop height and fixed potential energy of 45.13 N·m to measure the IDCPI. The IDCPIs of the five hammer weights were averaged at intervals of 5 cm as shown in Fig. 2. The DCP tests were also performed for comparison. The obtained DCPI was averaged at same intervals with the IDCPI. Fig. 2(a) shows the profiles of IDCPIs and DCPI according to the depth. To compare the penetration indices according to the boundary conditions, soils were classified as dense layer at the depth, where the DCPI was lower than 12 mm/blow, and loose layer at the depth, where the DCPI is more than 20 mm/blow. Except the depths of 650-750 mm, the soils in site A are classified as dense layers. The soils in sites B and C are classified as loose layers as shown in Figs. 2(b) and 2(c).

Then, the dynamic responses were obtained at stain-less steel plate as a fixed-end boundary condition and at loose soils, where the DCPI is more than 20 mm/blow, as a free-end boundary condition. Eleven types of hammer weight (4, 6, 8, 10, 12, 14, 16, 18, 20, 22, and 24 kg) were used with fixed potential energy (45.13 N·m) by adjusting the drop height.

Soil samples were collected in the field from three sites. The soil index properties were estimated and summarized in Table 1. Sieve analyses were conducted for samples in three sites based on ASTM D422 (2007). The effective diameters with 10%, 30%, 50%, and 60% passing percentage (D_{10}, D_{30}, D_{50}, and D_{60}) were obtained and the coefficients of uniformity (C_u) and curvature (C_c) were calculated using the effective diameters. Laboratory tests obtained specific gravities (G_s) were obtained by laboratory test according to ASTM D854 (2010). Finally, the samples from the three sites were classified as silty sands (SM) based on a unified soil classification system (USCS).

Table 1. Soil index properties in three sites.

Site	D_{10}	D_{30}	D_{50}	D_{60}	Cu	Cc	Gs	USCS
A	0.05	0.19	0.52	0.74	15.7	1.0	2.65	SM
B	0.04	0.10	0.46	0.77	18.9	0.3	2.65	
C	0.04	0.08	0.30	0.41	10.8	0.4	2.66	

*Unit of D_{10}, D_{30}, D_{50}, and D_{60} is 'mm'.

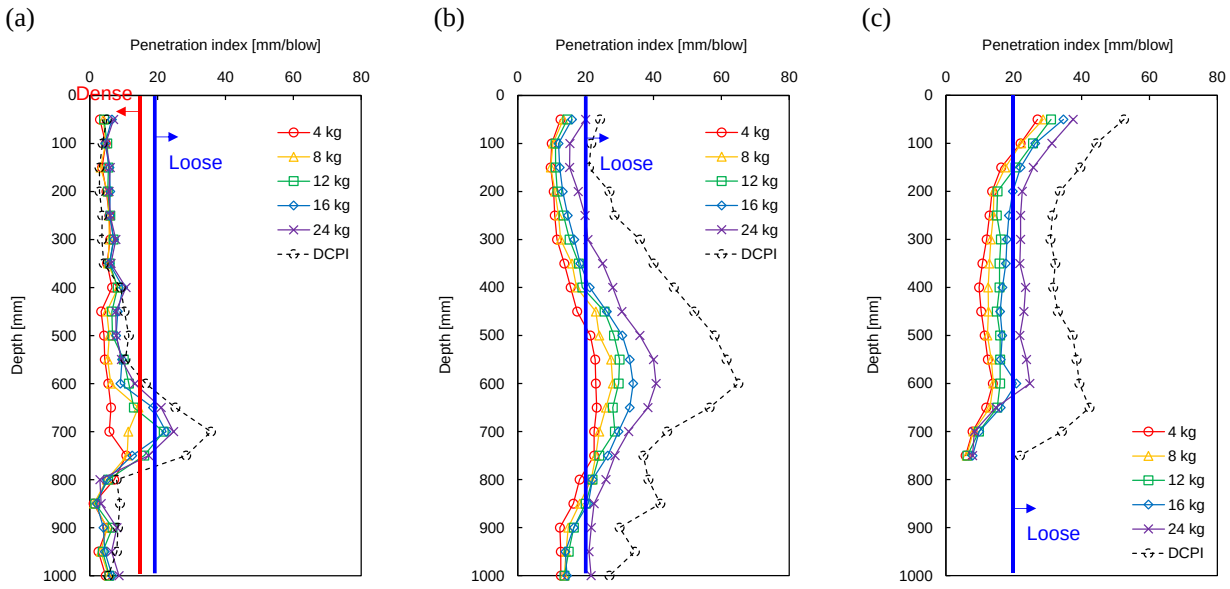

Figure 2. Profiles of penetration indices (IDCPI and DCPI) with hammer weights of 4, 8, 12, 16, and 24 kg.

3.2. Dynamic responses

A acceleration and force signals were obtained using the energy modules of the IDCP. The typical force- and energy-time waveforms are represented in Fig. 3. The force-time waveforms are measured from loadcell and accelerometer in the energy module (Fig. 3(a)). The value of first peak is considered to be the compression stress. The energy-time waveform is calculated as shown in Fig. 3(b). The transferred energy into the rod head or cone tip is calculated based on force-velocity integration method using the measured force (F_s) and calculated velocity (V_a) as follows:

$$E_{head} \ or \ E_{tip} = \int F_s \times V_a dt \qquad (4)$$

The force in Eq. (4), was measured using the loadcell, and the velocity was calculated from integral of acceleration measured using the accelerometer.

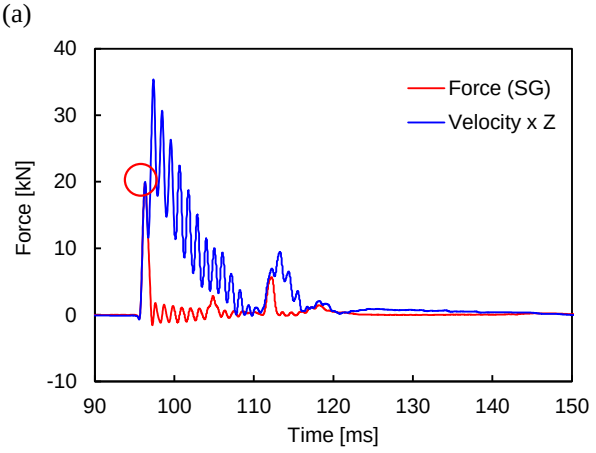

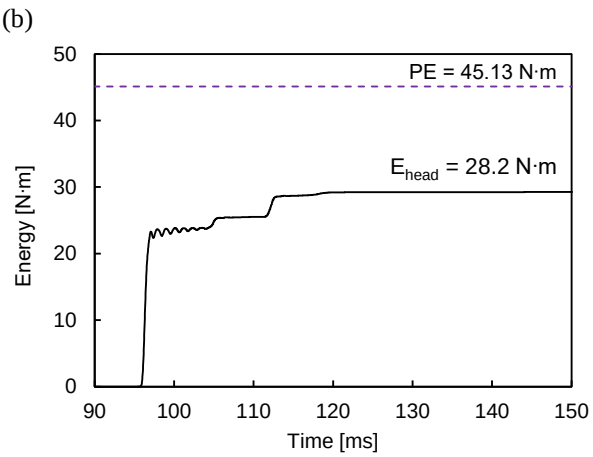

Figure 3. Typical dynamic responses: (a) force-time waveforms; (b) energy-time waveforms.

4. Experimental results and analyses

4.1. Penetration index

The obtained DCPI was correlated to the IDCPIs as shown in Fig. 4. The relationships between the DCPI and IDCPIs are separated according to the dense and loose layers in Figs. 4(a) and 4(b), respectively. The DCPI was larger than the IDCPIs because the diameter of the DCP was smaller than that of the IDCP. The IDCPI increases with the hammer weight in both layers. Gradients of relationship between the DCPI and IDCPI at dense layer are larger than those at loose layer. Note that larger gradient denotes that the IDCPI is more similar with the DCPI. Therefore, hammer weight and end boundary conditions affects the drivability of the IDCP. In other words, a heavier hammer weight and fixed-end boundary condition improve the drivability of dynamic penetrometer.

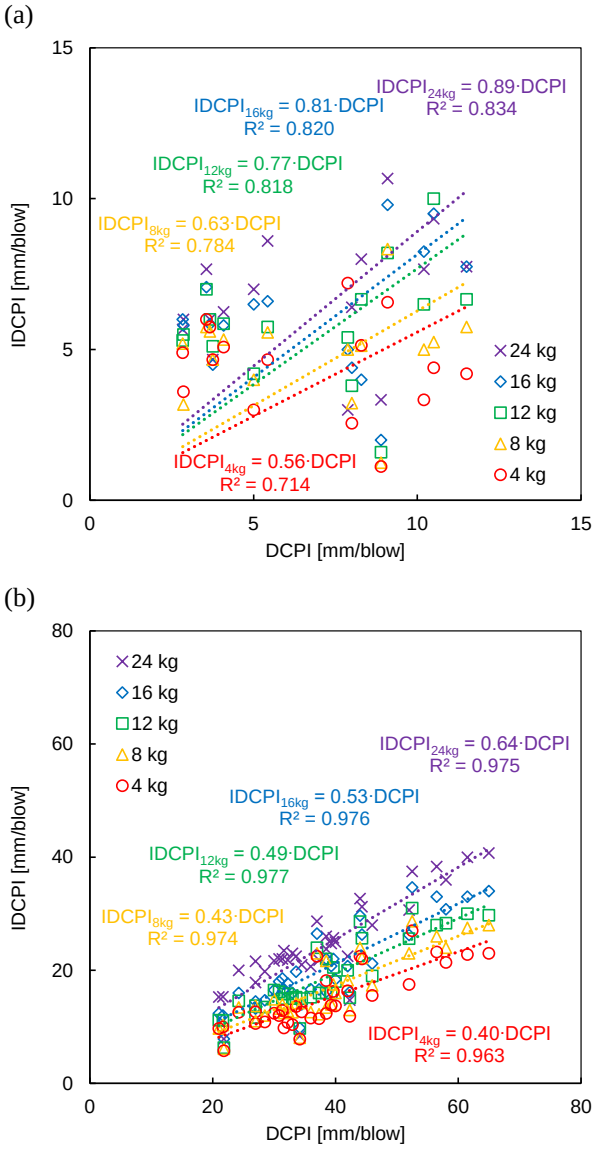

Figure 4. Relationships between penetration indices: (a) at dense layer; (b) at loose layer.

4.2. Transferred energy

The transferred energies into the rod head and cone tip were calculated based on Eq. (4) and plotted with hammer weight in Fig. 5. The relationships between the hammer weight and transferred energy into the rod head are represented in Fig. 5(a). Transferred energy into the rod head increases as the hammer weight increases. The relationships in the dense layer are similar to those in the loose layer. Thus, the transferred energy into the rod head is independent of end boundary condition. Fig. 5(b) shows the relationships between the hammer weight and transferred energy into the cone tip. The transferred energy into the cone tip increases with the hammer weight. The transferred energies into the cone tip at loose layer are smaller than those at dense layer. The difference decreases as the hammer weight increases. Therefore, the hammer weight affects the transferred energy into the cone tip.

The drop heights are plotted against the transferred energies as shown in Fig. 6. The transferred energies decrease as the drop height increases. The relationships between transferred energy into the rod head are represented in Fig. 6(a). Similar to hammer weight, the relationships between the drop height and transferred energy into the rod head is independent of end boundary condition. The relationships between the drop height and transferred energy into the cone tip are represented in Fig. 6(b). The transferred energies into the cone tip at dense layer are larger than those at loose layer.

Additionally, the difference in the transferred energy increases as hammer weight increases. According to Eq. (1), transferred energies increase as the drop height increases. However, drop height is adjusted with hammer weight, so it seems that transferred energy tends to decrease as drop height increase. In other words, transferred energy more depends on the hammer weight than the drop height. Lighter hammer weight and higher drop height may be more effected by air drag and friction between the hammer and guide rod.

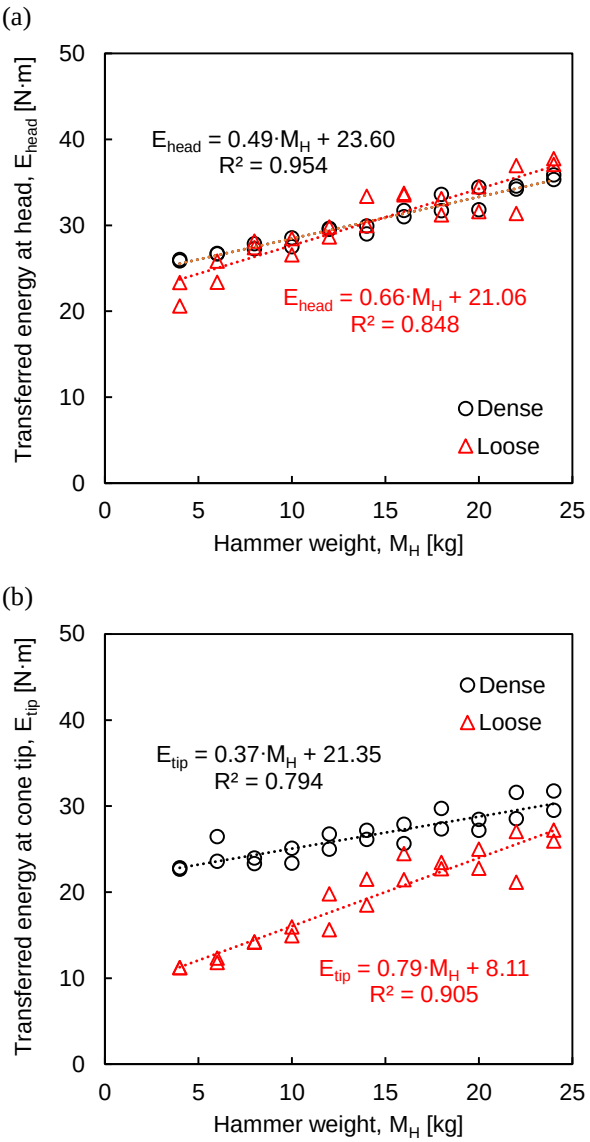

Figure 5. Relationship between hammer weight and transferred energies into: (a) rod head; (b) cone tip.

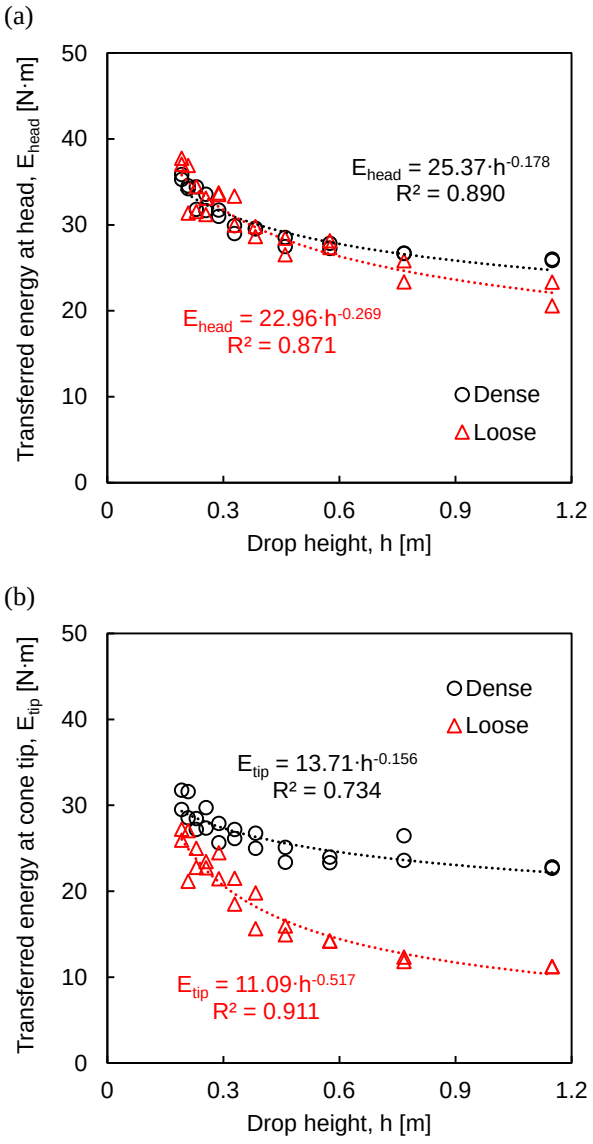

Figure 6. Relationships between drop height and transferred energies into: (a) rod head; (b) cone tip.

5. Conclusions

Dynamic responses were obtained using an instrumented dynamic cone penetrometer (IDCP) under fixed-end boundary condition (e.g., dense layer and stainless-steel plate) and free-end boundary condition (e.g., loose layer). The IDCP index (IDCPI) is compared with a dynamic cone penetration index (DCPI) in hammer weight of 4, 8, 12, 16, and 24 kg. Transferred energies at the rod head and cone tip are calculated by dynamic responses and plotted with eleven types of hammer weight and drop height (4-24 kg).

IDCPI is proportional to the DCPI with various gradients lower than 1 due to the low drivability of IDCP caused by larger diameter of cone. The gradient of relationship between the penetration indices increases with hammer weight. Heavier hammer weight in fixed-end boundary condition improves the drivability. The transferred energies into rod head and cone tip increase as hammer weight increases and drop height decrease. The hammer weight had a greater effects on the transferred energy than the drop height.

Acknowledgements

This work was supported by a National Research Foundation of Korea (NRF) grant funded by the Korean government (MSIT) (No. NRF-2021R1A5A1032433).

References

ASTM D422, 2007. *Standard test method for particle-size analysis of soils*, The American Society for Testing and Materials, West Conshohocken.

ASTM D854, 2010. *Standard test methods for specific gravity of soil solids by water pycnometer*, The American Society for Testing and Materials, West Conshohocken.

Burmister D. M. 1948. "The importance and practical use of relative density in soil mechanics." In Proceedings-American Society for Testing and Materials 48: 1249-68.

Byun, Y. H., Lee, J. S. 2013. "Instrumented dynamic cone penetrometer corrected with transferred energy into a cone tip: a laboratory study." Geotech Testing J 36, no. 4: 533–542. https://doi.org/10.1520/GTJ20120115.

George, V., Rao, N., Shivashankar, R. 2009. "Effect of soil parameters on dynamic cone penetration indices of laterite sub-grade soils from India." Geotech and Geological Eng 27, no.4: 585-593. https://doi.org/10.1007/s10706-008-9248-6.

Kim, S. Y., Lee, J. S. 2020. "Energy correction of dynamic cone penetration index for reliable evaluation of shear strength in frozen sand–silt mixtures." Acta Geotechnica 15, no. 4: 947-961. https://doi.org/10.1007/s11440-019-00812-y.

Lee, J. S., Byun, Y. H. 2020. "Instrumented cone penetrometer for dense layer characterization." Sensors 20, no. 20: 5782. https://doi.org/10.1520/GTJ20120115.

Malek G., Khamehchiyan M., Nikoudel M. R., Harsini K. M. 2020. "Horizontal Dynamic Cone Penetrometer: A New Device for Estimating Engineering Properties of Vertical Soil Wall in SP Soils." Geotech Testing J 44: 87-111. https://doi.org/10.1520/GTJ20180319.

Park, G., Kim, N., Kang, S., Kim, S. Y., Yoo, C., Lee, J. S. 2022. "Instrumented dynamic cone penetrometer incorporated with time domain reflectometry." Measurement 206: 112337. https://doi.org/10.1016/j.measurement.2022.112337.

Youd, T. L., Bartholomew, H. W., Steidl, J. H. 2008. "SPT hammer energy ratio versus drop height." J of Geotech and Geoenv Eng 134, no. 3: 397-400. https://doi.org/10.1061/(ASCE)1090-0241(2008)134:3(397).